Korean J. Chem. Eng., 40(3), 548-554 (2023)
DOI: 10.1007/s11814-022-1360-4

pISSN: 0256-1115
eISSN: 1975-7220

Selective outer surface modification of polycrystalline Ni-rich cathode for sulfide all-solid-state lithium-ion battery

Jae Hong Choi*, Junhyeok Hwang, Tom James Embleton*, Kyungmok Ko*, Mina Jo*, Chaewon Lee*, Jeongsik Yun*, Seohyeon Park*, Yoonkook Son***, and Pilgun Oh*,**,†**

*Department of Smart Green Technology Engineering,
**Department of Nanotechnology Engineering, Pukyong National University, 45, Yongso-ro, Nam-gu, Busan 48547, Korea
***Department of Electrical Engineering, Chosun University, 309 Pilmun-daero, Dong-gu, Gwangju 61452, Korea
(*Received 2 September 2022 • Revised 15 November 2022 • Accepted 30 November 2022*)

Abstract−In order to achieve a high energy density, Ni-rich polycrystalline materials have been explored as cathode materials for application in ASSLB applying sulfide solid electrolyte. However, the interaction between the electrode and the solid electrolyte comes with severe problems, such as a poor solid electrolyte interface and interfacial stress fracturing during the charge-discharge process. To alleviate the side reaction and the interfacial resistance, a coating layer between the cathode and sulfide electrolyte has since been proposed and developed. However, the inner surface of the primary particles in the polycrystalline can also be a form of coating layer, which does not meet the solid electrolyte and it is hence an inefficient coating mechanism for an ASSLB where the cathode/electrolyte interface occurs purely at the cathode outer surface. Here, we report a new coating strategy for Ni-rich polycrystalline cathode materials using a sol-gel process that focusses on improving the cathode/electrolyte interface of ASSLB. Commercial polycrystalline $LiNi_{0.8}Co_{0.1}Mn_{0.1}O_2$ was coated with 1 wt% lithium and cobalt acetate precursor with different coating coverage being achieved via control of the stirring speed (200 and 600 rpm). The coating materials, which uniformly coated on the inner and outer surfaces of the polycrystalline (I-NCM), showed effectively improved electrochemical performance with the structural stability in LIB, where the liquid electrolyte has contact with inner surface of polycrystalline materials. However, the cathode material, which was mainly coated on the outer surface of polycrystalline materials (O-NCM), exhibited improved performance in the ASSLB, which only has contact with the electrolyte at the surface of the active material polycrystalline. The physical properties of the coated cathode material were analyzed using SEM and XRD, and the electrochemical performance was investigated through initial charge/discharge capacity and cycle stability in both LIB and ASSLB simultaneously. This concept of intentionally surface coating the polycrystalline material can be applied as a new coating strategy to realize improvements in both electrochemical properties and electrode structural stability of ASSLB.

Keywords: All-solid-state Batteries, Polycrystalline Ni-rich Cathode Materials, Precursor Coverage Control, Sulfide Electrolytes, Surface Modification, Coating

INTRODUCTION

Lithium-ion batteries (LIB) are the current dominant energy storage systems with properties such as light weight, high energy density, high capacity, and high-efficiency granting them the top spot. Their impressive power supply can be applied in relatively small applications like portable electronics to large-scale applications such as electric vehicles and even ultra-large-scale application such as stationary energy storage systems [1-3]. Conventional LIBs that use highly volatile and flammable organic solvents as electrolytes have advantages such as small size, no memory effect [4], and long cycle life [5], but have safety issues under particularly harsh operating conditions [5]. Hence, all-solid-state lithium-ion batteries (ASSLB) are considered a next-generation device for energy storage composed of inorganic solid materials with high electrochemical and thermal stability, and improved energy and power density [6]. Research on ASSLBs has been increasing as solid electrolytes with high ion conductivity have been reported, allowing researchers to focus on other issues [7,8].

The most decisive factor in determining the price and performance of LIB and ASSLB is the cathode material, and hence cathode material research is being actively conducted to achieve the performance required in the market. In the case of $LiCoO_2$ material, which led to the commercialization of lithium-ion batteries, despite having a high theoretical capacity of 272 mAh/g [9], there is a limitation to realizing high-energy batteries due to the low achievable discharge capacity of ~140 mAh/g across the 3.6-4.2 V range [10]. Because of the low energy density of $LiCoO_2$, alternate materials have been suggested. High-Ni cathode materials, such as $LiNi_xM1_yM2_{1-x-y}O_2$ (M=Co, Mn, etc.; x>0.5), have come into focus due to their high energy density, large voltage stability range and high achievable capacity [11,12]. By increasing the Ni content in the cathode material, both price and performance are satisfied as the expensive Co content is lowered and the capacity is increased.

†To whom correspondence should be addressed.
E-mail: poh@pknu.ac.kr

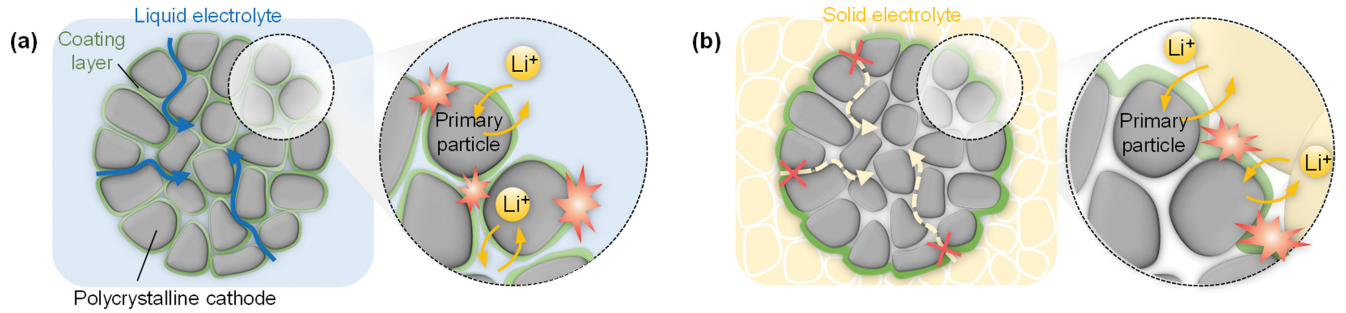

Fig. 1. Scheme of coating strategy for polycrystalline cathode in (a) lithium-ion batteries (LIB) and (b) all-solid-state lithium-ion batteries (ASSLB).

However, the Ni-rich cathode has structural and electrochemical instability limitations, which are exacerbated by increasing the Ni content in the material to achieve a higher capacity. One of the known limitations of Ni-rich material is cation mixing where originally layered phase ($R\bar{3}m$) Ni-rich cathode materials are changed to spinel-like phase ($Fd\bar{3}m$) and rock-salt phase ($Fm\bar{3}m$) due to the migration of the transition metal (TM) ions into lithium layer during charge and discharging [13,14]. To overcome these limitations, research on surface modification (coating) and element substitution (doping) are primarily being conducted. Among these two stabilizing techniques, surface modification is known to more affect the interfacial performance, whereas ion substitution generally alters the internal structural stabilization of the cathode material [15].

Ni-rich cathode materials are composed of micrometer-sized polycrystalline in which many 0.1-1 μm-sized primary particles (grains) are aggregated [16,17]. Regarding polycrystalline, the three-dimensional hierarchical aggregate of primary particles leads to the formation of grain boundaries of different crystallographic orientation that allow the permeation of liquid electrolyte [18]. Therefore, there is contact with the electrolyte of LIB not only on the outer surface but also the inner surface of the polycrystalline (Fig. 1(a)). In consequence, the side reactions of the Ni-rich cathode material with the electrolyte during the cycle are severe, such as complicated composition of the solid electrolyte interphase (SEI) layer [19], erosion of the surface structure [20] and dissolution of TM ions by the HF attack mechanism [21]. Therefore, coating of the entire outer surface of the polycrystalline, including the individual primary particles, is the most effective method to suppress side reactions via liquid electrolyte [22,23].

To achieve high energy density, Ni-rich polycrystalline materials, such as $LiNi_{1/3}Co_{1/3}Mn_{1/3}O_2$, $LiNi_{0.8}Co_{0.15}Al_{0.05}O_2$ and $LiNi_{0.5}Mn_{0.15}O_4$, have been explored as cathode materials in ASSLB with sulfide solid electrolyte [12,27-30]. The key challenges in the development of cathode materials for high energy ASSLBs are a poor SEI caused from side reaction at interface between the active material and the solid electrolyte (SE) [24,25], and interfacial stress during the charge-discharge process caused by volume changes in the active material [26]. To alleviate the side reaction and the interface resistance, $LiNbO_3$ [12], ZrO_2 [27], $LiAlO_2$ [28], $Li_4Ti_5O_{12}$ [29] and Li_2-ZrO_2 [30] have been applied as a coating layer between cathode and sulfide electrolyte. Considering that the contact of the solid electrolyte is formed on the outer surface of the active material in ASSLB, the coating layers on the cathode materials should be primarily formed on the outer surface to obtain the desired alleviation of the interfacial issues (Fig. 1(b)), while minimizing the change in the electrochemical and structural properties of the cathode material. However, techniques to achieve this focused surface-only coating of active material for ASSLB application have not been commonly analyzed using the sol-gel method, which is the liquid-based process and is suitable for mass production. Taking this into consideration, developing a coating method that is both suitable for mass production and can form a coating layer focused to the outer surface of the polycrystalline cathode is vital for the development of ASSLB as a whole.

In this paper, we propose a coating strategy of Ni-rich polycrystalline cathode materials for ASSLBs using cheap lithium and cobalt acetate precursors and applying a scalable sol-gel process. Commercial polycrystalline $LiNi_{0.8}Co_{0.1}Mn_{0.1}O_2$ was coated by 1 wt% lithium and cobalt acetate precursor dissolved in ethanol solution with a different precursor coating coverage being achieved by altering the stirring speed (200 and 600 rpm). When the stirring speed was 200 rpm, the lithium and cobalt precursors were uniformly adsorbed on the inner and outer surface of the polycrystalline cathode and formed a coating layer over the primary particles that make of the polycrystalline. This sample (I-NCM) showed a relatively enhanced cycle property in the LIB. On the other hand, when the stirring speed was increased to 600 rpm, the precursors were mainly adsorbed on the polycrystalline outer surface and formed a coating layer over the outer surface of the sample. This sample (O-NCM) showed relatively enhanced cycle performance when applied in the ASSLB. The physical properties of the coated cathode material were analyzed using SEM and XRD, and the electrochemical performance was investigated through initial charge/discharge capacity and cycle stability through both LIB and ASSLB evaluation.

EXPERIMENTAL

1. Surface Modification Method

Pristine $LiNi_{0.8}Co_{0.1}Mn_{0.1}O_2$ was obtained from POSCO chemical for surface modification, with $Li(CH_3COO)\cdot 2H_2O$ and $Co(CH_3COO)\cdot 4H_2O$ (Sigma Aldrich). A typical sol-gel surface modification method was applied to the coating process. The acetate precursors applied for coating (Li & Co) of calculated weight for 1 wt% coating of $LiNi_{0.8}Co_{0.1}Mn_{0.1}O_2$ were fully dissolved in an anhydrous ethanol

solvent (7 g) and mixed at 200 rpm and 600 rpm until fully dissolved. 1 g of the pre-prepared $LiNi_{0.8}Co_{0.1}Mn_{0.1}O_2$ sample was added, and the applied heating temperature was increased to 120 °C. The samples were held at such conditions until the ethanol solvent had fully evaporated. The samples were then dried at 150 °C for two hours in a standard oven, before being annealed at 800 °C in an O_2 atmosphere for four hours.

2. Electrochemical Characterization Method of LIB

The cathode electrode composite was comprised of an active material ($LiNi_{0.8}Co_{0.1}Mn_{0.1}O_2$), poly vinylidene fluoride (PVDF) binder and Super P as the conductive material in a ratio of 92 : 4 : 4. The cathode electrode was then made via doctor blade manual casting onto aluminum foil with the active material loading at ~6-7 $mg{\cdot}cm^{-2}$. The electrolyte used was 1.3 M $LiPF_6$ in EC/EMC/DEC (=3/5/2, v/v/v)+10% FEC+0.5% VC+1% PS+0.2% $LiBF_4$. The electrochemical data was attained via half-cell coin cell testing (2032R). The galvanostatic cycling conditions applied for the formation cycle were 0.1 C and voltage range 2.7-4.3 V, with the C rate being increased to 1 C after the formation cycle and the other conditions remaining the same. The temperature of all formation and cycling tests was 30 °C.

3. Electrochemical Measurements of ASSLB

The pristine $LiNi_{0.8}Co_{0.1}Mn_{0.1}O_2$ and surface modified cathodes were synthesized into a cathode composite powder which was mixed with Li_6PS_5Cl solid electrolyte in weight ratio of 7 : 3 using an agate mortar as the composite cathode. Li-In was mixed at a ratio of 3 : 97 and SE was additionally mixed at a ratio of 4 : 1, with Li-In-SE as a counter electrode. ASSLBs were assembled as follows: 150 mg Li_6PS_5Cl solid electrolyte was pressed under 10 MPa into an electrolyte layer with 13 mm in diameter. Then, 15 mg of the above composite cathode powder was uniformly spread on one side of the electrolyte layer and a stainless-steel electrode cap was put on composite cathode layer. Next, 35 mg of the Li/In mixture was uniformly spread on the other side of electrolyte layer, and Ni foil was covered thereon. Finally, all the components were compressed together under 40 MPa to form the final ASSLB.

4. Characterization Method

Powder X-ray diffraction (XRD) data was analyzed via D/Max2000, Rigaku. The measurements were taken between 2θ= 10-80° with radiation from source Cu Kα radiation. A scanning electron microscope (SEM) TESCAN (VEGA II LSU) was used to identify the sample morphology and degradation occurring on the surface and internally in back-scattered electron (BSE) mode. The cross-section SEM images were attained by first ion-milling the samples with Gatan (697 Ilion II) system.

RESULTS AND DISCUSSION

The overall morphology of the cathode materials before and after precursor coating was initially analyzed by SEM. The SEM images of bare $LiNi_{0.8}Co_{0.1}Mn_{0.1}O_2$ (NCM) showed a polycrystalline morphology with a clean surface made up of pseudo-round-shaped, tightly packed, nanoscale primary particles (Fig. 2(a)). When lithium and cobalt acetate precursor were coated on the NCM surface using the sol-gel process, these precursors were adsorbed onto the NCM surface and well penetrated into grain boundaries of the polycrystalline, as these precursors are well dissolved in the ethanol solvent [22]. When the rotational mixing speed of the sol-gel process was low (200 rpm), the evaporation speed of the solvent was relatively slow, and the time taken for these precursors to penetrate between the primary particles was extended. When the string speed was 200 rpm during the sol-gel process with these precursors, a relatively small number of precursors were adsorbed on the surface of the cathode material (Fig. 2(b)) because these precursors were uniformly adsorbed on inner and outer surface (I-NCM). As a result, the coated cathode materials have a morphology with low precursor coverage on the surface. Conversely, when the stirring speed increased, the evaporation speed of the solvent increased, so

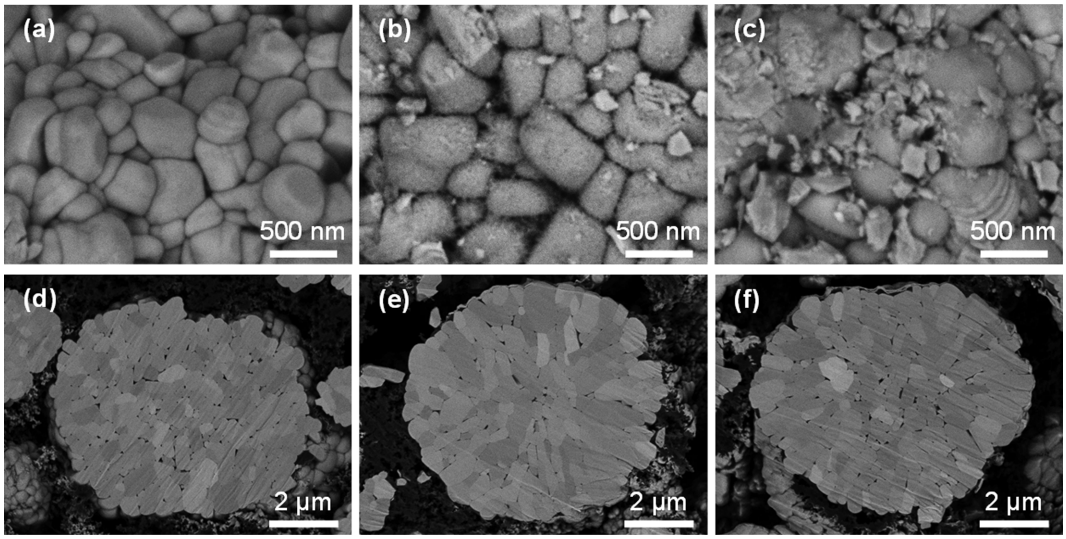

Fig. 2. Scanning electron microscope (SEM) image of (a) bare $LiNi_{0.8}Co_{0.1}Mn_{0.1}O_2$ (NCM), (b) Li and Co acetate precursor coated NCM with low coverage (I-NCM) and (c) Li and Co acetate precursor coated NCM with high coverage (O-NCM) before heat treatment. Cross-sectional SEM images of (d) bare NCM, (e) I-NCM and (f) O-NCM after 800 °C heat treatment.

these precursors did not have sufficient time for extended penetration between the primary particles. The coated cathode material applying the sol-gel process at a high stirring speed of 600 rpm (O-NCM, Fig. 2(c)) showed a high precursor concentration on outer surface of the polycrystalline. This simple change to the sol-gel process results in entirely different morphology, and allows for tailoring of the coating layer based on the intended battery system of future application. Additionally, when the lithium and cobalt acetate precursor is coated onto the primary particles which are internal to the polycrystalline material, it leads to a decrease in the internal void ratio [22]. When the color ratio was calculated, which means void space in the polycrystalline from the cross-section SEM image is analyzed via image processing, the internal void ratio of bare is approximately 0.13%. As shown in the Fig. 2(b)-(c), which presents cross-sectional images after 800 °C calcination with lithium and cobalt precursors, the internal void ratio of I-NCM is approximately 0.05%, which is significantly lower than the bare. This means that a coating layer was formed throughout the primary particles inside the polycrystalline via the lithium and cobalt precursors. In the case of O-NCM, the internal porosity was approximately 0.12%, similar to that of bare NCM. That is, a coating layer by lithium and cobalt acetate was formed on the outer and inner surfaces of the polycrystalline materials in the case of I-NCM, and a coating layer was mainly formed on the outside of the polycrystalline in the case of O-NCM.

The X-ray diffraction analysis of bare NCM, I-NCM and O-NCM recorded at a scan speed of 3° min^{-1} in a 2θ range of 10-80° is shown in Fig. 3(a). A cathode material that has lower than 1.40 for $I_{(003)}/I_{(104)}$ has cation mixing characteristics, which indicates an instability within the layered structure that results in Ni^{2+} ions preventing the diffusion of the Li^{+} ions during the charge/discharge process [31]. The $I_{(003)}/I_{(104)}$ combined with clear peak splitting of (006), (102) (108), and (110) planes indicates that a layered structure is well developed [32]. The R-factor expressed as the value of

Table 1. $I_{(003)}/I_{(104)}$ and R-factor values of Bare NCM, I-NCM and O-NCM. The values are obtained from XRD data of Fig. 2

	R-factor	$I_{(003)}/I_{(104)}$
Bare NCM	0.44	1.68
I-NCM	0.48	1.57
O-NCM	0.48	1.34

$(I_{(102)}+I_{(006)})/I_{(101)}$ indicates the hexagonal ordering of the material [31]. When the R-factor value has a value of 0.41-0.5, it indicates the cathode material has low degree of cation mixing with high crystallinity [31]. The $I_{(003)}/I_{(104)}$ and the R-factor of bare NCM are 1.68 and 0.44 (Table 1), respectively, with clear peak splitting of (006), (102) (108), and (110) planes (Fig. 3(b)-(c)), indicating the bare NCM has a low degree of cation mixing as expected. The $I_{(003)}/I_{(104)}$ and the R-factor of I-NCM is 1.57 and 0.48 and that of O-NCM is 1.34 and 0.48. Both I-NCM and O-NCM showed clear peak splitting of (006), (102) (108), and (110) planes. Considering $I_{(003)}/I_{(104)}$, R-factor and the peak splitting of (006), (102) (108), and (110) planes, it is concluded that cation mixing barely occurred in the I-NCM and O-NCM after lithium and cobalt coating.

The electrochemical properties of the LIB were evaluated to compare the initial discharge capacity and cycle properties of bare NCM, I-NCM and O-NCM. As shown in Fig. 4(a), the bare NCM, I-NCM and O-NCM exhibits a charge capacity of 225.2, 218.8 and 222.2 mAh/g, a discharge capacity of 202.9, 195.7 and 199.7 mAh/g and an initial coulombic efficiency (ICE) of 91.7%, 89.5% and 89.9% in LIB evaluation within the voltage range of 2.7-4.3 V, respectively (Table 2). The I-NCM and O-NCM show lower discharge capacity and ICE than the bare NCM due to a lack of electrons on the surface of the active material after oxide coating [33,34]. The I-NCM and O-NCM exhibit a lower overpotential than bare NCM during the charge process of the initial charge/discharge. Importantly, the electrochemical characteristics of the coated samples were

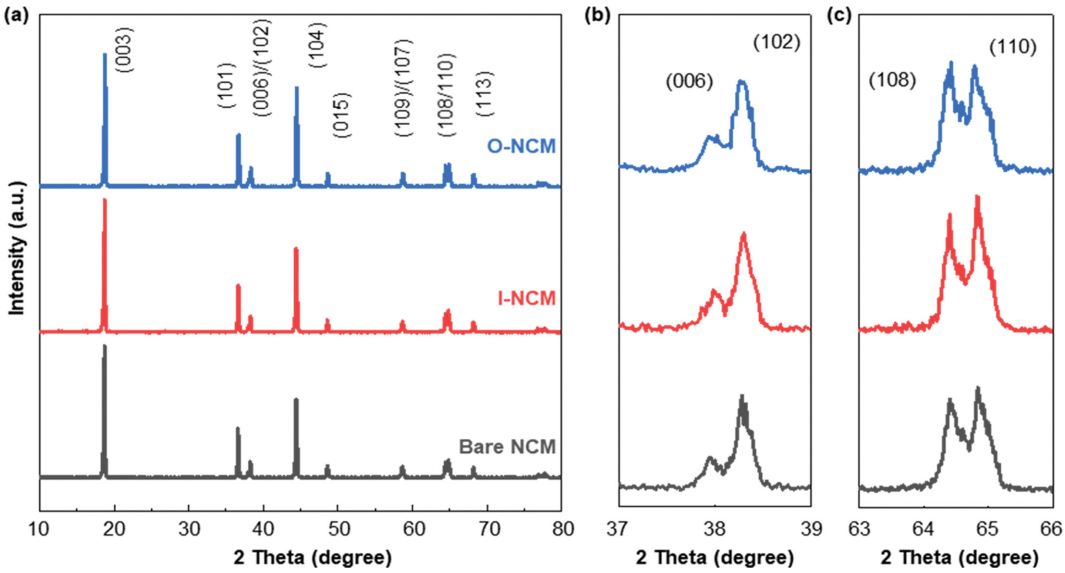

Fig. 3. (a) X-ray diffraction (XRD) patterns of the bare NCM, I-NCM and O-NCM after 800 °C heat treatment in O_2. (b) A zoomed-in view of 2 theta (37-39 degrees) and (c) (63-66 degrees).

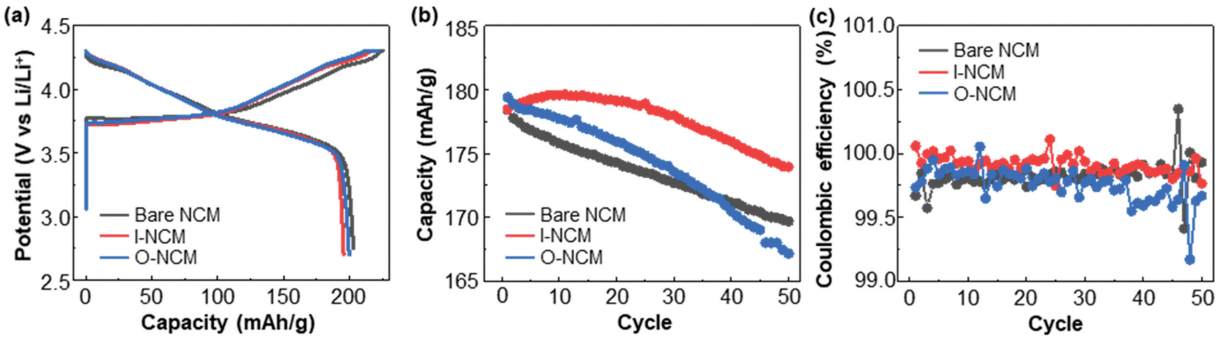

Fig. 4. Electrochemical performance of Bare NCM, I-NCM and O-NCM in LIB (a) Initial charge-discharge voltage profiles of at 0.1 C rate between 3.0 and 4.3 V at 30 °C. (b) Cycle performance and (c) Coulombic efficiency with charge and discharge C-rates of 1 C.

Table 2. Charge capacity, discharge capacity and initial coulombic efficiency (ICE) of bare NCM, I-NCM and O-NCM at 0.1 C rate. Discharge capacity of 1st cycle and capacity retention after 50 cycles at 1 C. These values were obtained in LIB

	Charge capacity (mAh/g)	Discharge capacity (mAh/g)	ICE (%)	1st discharge capacity (mAh/g)	Capacity retention @ 50 cycle (%)
Bare NCM	225.2	202.9	91.7	178.4	95.1
I-NCM	218.8	195.7	89.5	178.4	97.5
O-NCM	222.2	199.7	89.9	179.4	93.2

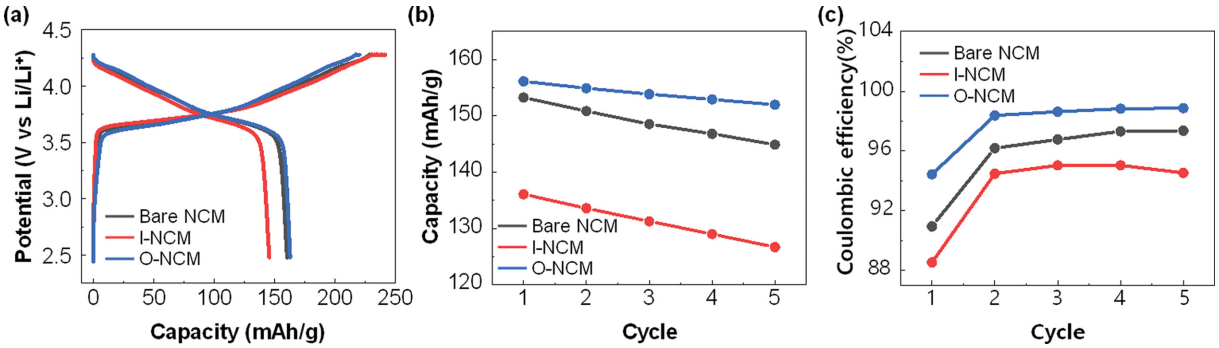

Fig. 5. Electrochemical performance of Bare NCM, I-NCM and O-NCM in sulfide ASSLB (a) Initial charge-discharge voltage profiles of at 0.05 C rate between 3.0 and 4.3 V at 30 °C. (b) Cycle performance and (c) coulombic efficiency with charge and discharge C-rates of 0.5 C.

Table 3. Charge capacity, discharge capacity and initial coulombic efficiency (ICE) of bare NCM, I-NCM and O-NCM at 0.1 C rate. Discharge capacity of 1st cycle and capacity retention after 50 cycles at 0.5 C. These values were obtained in sulfide ASSLB

	Charge capacity (mAh/g)	Discharge capacity (mAh/g)	ICE (%)	1st discharge capacity (mAh/g)	Capacity retention @ 50 cycle (%)
Bare NCM	235.2	160.4	68.2	153.3	94.5
I-NCM	241.6	145.6	60.2	136.1	93.1
O-NCM	220.0	162.8	74.0	156.1	97.3

minimally affected during the formation cycle; however, significant differences are observed during the cycling evaluation (Fig. 4(b)). The I-NCM with increased discharge capacity up to 10 cycles [35] exhibits an improved retention of 97.5% at 50 cycles compared to that of the bare NCM (95.1%). The O-NCM also shows improved discharge capacity in the beginning of the cycle measurements, but the cycle retention is lower than bare after 50 cycles. In terms of Columbic efficiency (Fig. 4(c)), the I-NCM exhibits a higher value than bare NCM and O-NCM on average. Considering the initial charge/discharge capacity, cycle properties, and coulombic efficiency in the LIB evaluation, a coating mechanism capable of coating all parts, internal and external, of the polycrystalline such as that of the I-NCM sample should be applied for the coating effect to be suited to a LIB.

Interestingly, the coating coverage required for improving electrochemical performance in LIBs and in ASSLBs is different. As

shown in Fig. 5(a), the I-NCM samples exhibit lower discharge capacity and ICE than the bare NCM during the ASSLB evaluation within the voltage same voltage range of 2.7-4.3 V (Table 3). However, in the case of O-NCM, where the precursor mainly formed a coating layer on the outer surface of the polycrystalline, the discharge capacity was 162.8 mAh/g and ICE was 74%. The value of O-NCM is higher than that of bare NCM. The O-NCM also exhibits improved cycle properties when compared to the bare NCM in the voltage range of 2.7-4.3 V (Fig. 5(b)). The discharge capacity of the 1st cycle of O-NCM is 156.1 mAh/g and the retention at the 5th cycle is 97.3%, which is higher than the average discharge capacity of bare during all five cycles. On the other hand, in the case of I-NCM, the discharge capacity of the 1st cycle is 145.6 mAh/g and the retention of the 5th cycle is 93.1%, the electrochemical performance after coating is greatly reduced. Also, the O-NCM exhibits a Columbic efficiency higher than the bare during the cycle evaluation (Fig. 5(c)). When considering all of the electrochemical analysis and the cumulative performance of the samples, O-NCM, in which much of the precursor was coated on the polycrystalline outer surface, exhibits a dominant improvement over the bare sample with the initial discharge capacity, ICE, cycle properties and coulombic efficiency all being increased. This indicates that coating the outer surface of polycrystalline cathode material is most suitable when applied in an ASSLB due to its ability to buffer against contact with the solid electrolyte which remains purely at the polycrystalline surface.

Differential capacity (dQ/dV) curves were analyzed to better understand the different charge and discharge properties of bare NCM, I-NCM and O-NCM (Fig. 6). All curves display three couples of redox peaks due to the phase transitions from hexagonal (H1) to monoclinic (M), monoclinic (M) to hexagonal (H2), and hexagonal (H2) to hexagonal (H3) during delithiation and lithiation processes [36]. Fig. 6(a)-(c) show the dQ/dV curves of bare NCM, I-NCM and O-NCM from the LIB evaluation. As shown in Fig. 5(a), the bare NCM shows an H1-M peak at a non-constant voltage and the H2-H3 peak is shifted to significantly higher potential during cycling. The I-NCM shows stable reversibility of the H1-M and H2-H3 phase transition (Fig. 6(b)) compared to the O-NCM, which shows the shifts of H1-M and H2-H3 peaks (Fig. 6(c)). However, a different trend was observed for the dQ/dV curves from the ASSLB evaluation. As shown Fig. 6(d)-(f), the bare NCM (Fig. 6(d)) and I-NCM (Fig 6(e)) exhibit a peak shift over the H1-M and H2-H3 ranges, with the intensities of these peaks greatly decreasing over the five cycles, corresponding to their decrease in capacity over the ASSLB cycle evaluation. However, the peak positions of H1-M and H2-H3 are almost identical over the five cycles in the dQ/dV curve of O-NCM (Fig. 6(f)) and the peak intensity and hence capacity was reasonably well maintained. In conclusion, the I-NCM, in which lithium and cobalt precursor coated the internal and external surfaces of the polycrystalline, exhibit stable reversibility of the H1-M and H2-H3 phase transition during the LIB evaluation. However, in the ASSLB evaluation, O-NCM, primarily coated with lithium and cobalt on the outer surface of the polycrystalline, shows enhanced reversibility of the H1-M and H2-H3 phase transition.

CONCLUSION

$LiNi_{0.8}Co_{0.1}Mn_{0.1}O_2$ cathode material, which was mainly coated with lithium and cobalt acetate precursor of 1 wt% on the outer surface of the polycrystalline (O-NCM), was prepared for enhanced performance in the ASSLB. These acetate precursors, which can easily penetrate the core part of polycrystalline, were strategically placed at the outer surface of the polycrystalline material by con-

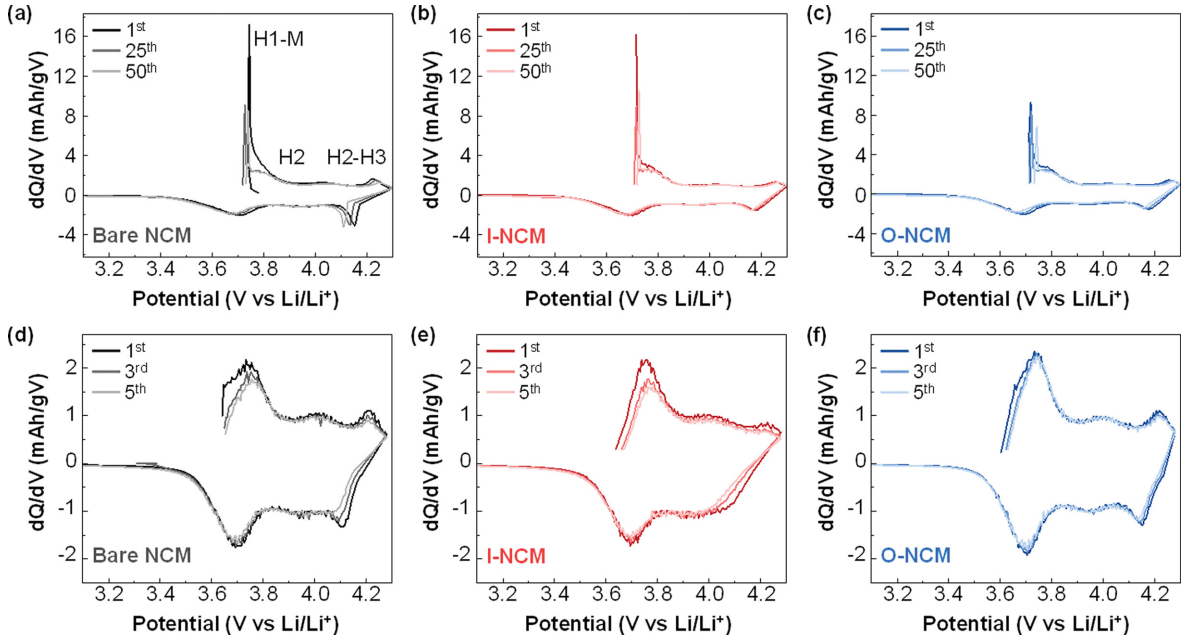

Fig. 6. Differential capacity curves of the bare NCM, I-NCM and O-NCM in (a)-(c) LIB and (d)-(f) ASSLB. These data are corresponding to Fig. 4(b) and Fig. 5(b), respectively.

trolling the stirring speed during sol-gel process. The cross-section SEM images, which exhibited the ratio of the internal void similar to that of bare combined with surface SEM images, confirmed that these precursors were highly adsorbed on the outer surface of the NCM active material. To compare the coating effect of O-NCM according to the selective site adsorption of the precursor, I-NCM samples, which were coated on the inner and outer surfaces of the primary particles of the polycrystalline, were prepared through a low stirring speed sol-gel process and evaluated simultaneously in LIB and ASSLB. In the LIB evaluation, where the liquid electrolyte has contact with inner primary particles of the polycrystalline, the I-NCM sample showed effectively improved electrochemical performance with enhanced structural stability, but there was no performance improvement in O-NCM. In contrast, O-NCM exhibited improved performance in the evaluation of the ASSLB, which has contact strictly on the surface polycrystalline material with the solid electrolyte. This concept of intentionally surface coating Ni-rich polycrystalline material for application is ASSLB can be applied as a new coating strategy to realize improvements in both the electrochemical properties and the structural stability of the cathode electrode. This paper highlights the importance of specifying the target-use battery system and developing strategic coating techniques that are suitable to the physical and chemical characteristics of the chosen configuration.

ACKNOWLEDGEMENTS

This research was supported by the Basic Research Program through the National Research Foundation of Korea (NRF) funded by the MSIT (2020R1A4A1019463) and by Basic Science Research Program through the National Research Foundation of Korea (NRF) funded by the Ministry of Education (2021R1A6A3A01088221, 2022R1I1A3069172). It was also supported by the Korea Institute of Energy Technology Evaluation and Planning (KETEP) grant funded by the Korea government (MOTIE) (20221B1010003B, Integrated High-Quality Technology Development of Remanufacturing Spent Cathode for Low Carbon Resource Recirculation).

CONFLICT OF INTEREST

The authors declare no conflict of interest.

REFERENCES

1. Y. Nishi, *J. Power Sources*, **100**, 101 (2001).
2. J.-M. Tarascon and M. Armand, *Nature*, **414**, 359 (2001).
3. A. Manthiram, *ACS Cent. Sci.*, **3**, 1063 (2017).
4. T. Sasaki, Y. Ukyo and P. Novák, *Nat. Mater.*, **12**, 569 (2013).
5. M. S. Whittingham, *Chem. Rev.*, **104**, 4271 (2004).
6. J. Janek and W. G. Zeier, *Nat. Energy*, **1**, 1 (2016).
7. W. Zhang, D. A. Weber, H. Weigand, T. Arlt, I. Manke, D. Schröder, R. Koerver, T. Leichtweiss, P. Hartmann and W. G. Zeier, *ACS Appl. Mater. Interfaces*, **9**, 17835 (2017).
8. C. Wang, J. Liang, Y. Zhao, M. Zheng, X. Li and X. Sun, *Energy Environ. Sci.*, **14**, 2577 (2021).
9. C. M. Julien, A. Mauger, K. Zaghib and H. Groult, *Inorganics*, **2**, 132 (2014).
10. A. Zhou, X. Dai, Y. Lu, Q. Wang, M. Fu and J. Li, *ACS Appl. Mater. Interfaces*, **8**, 34123 (2016).
11. G. Peng, X. Yao, H. Wan, B. Huang, J. Yin, F. Ding and X. Xu, *J. Power Sources*, **307**, 724 (2016).
12. X. Li, L. Jin, D. Song, H. Zhang, X. Shi, Z. Wang, L. Zhang and L. Zhu, *J. Energy Chem.*, **40**, 39 (2020).
13. F. Lin, I. M. Markus, D. Nordlund, T.-C. Weng, M. D. Asta, H. L. Xin and M. M. Doeff, *Nat. Commun.*, **5**, 1 (2014).
14. G. Sun, X. Yin, W. Yang, A. Song, C. Jia, W. Yang, Q. Du, Z. Ma and G. Shao, *Phys. Chem. Chem. Phys.*, **19**, 29886 (2017).
15. W. Yan, S. Yang, Y. Huang, Y. Yang and G. Yuan, *J. Alloys Compd.*, **819**, 153048 (2020).
16. X. Fan, G. Hu, B. Zhang, X. Ou, J. Zhang, W. Zhao, H. Jia, L. Zou, P. Li and Y. Yang, *Nano Energy*, **70**, 104450 (2020).
17. Y. Xia, J. Zheng, C. Wang and M. Gu, *Nano Energy*, **49**, 434 (2018).
18. L. Zou, W. Zhao, H. Jia, J. Zheng, L. Li, D. P. Abraham, G. Chen, J. R. Croy, J.-G. Zhang and C. Wang, *Chem. Mater.*, **32**, 2884 (2020).
19. D. Hu, Y. Su, L. Chen, N. Li, L. Bao, Y. Lu, Q. Zhang, J. Wang, S. Chen and F. Wu, *J. Energy Chem.*, **58**, 1 (2021).
20. Z. Zhang, P. Zhou, H. Meng, C. Chen, F. Cheng, Z. Tao and J. Chen, *J. Energy Chem.*, **26**, 481 (2017).
21. S. Chen, T. He, Y. Su, Y. Lu, L. Bao, L. Chen, Q. Zhang, J. Wang, R. Chen and F. Wu, *ACS Appl. Mater. Interfaces*, **9**, 29732 (2017).
22. H. Kim, M. G. Kim, H. Y. Jeong, H. Nam and J. Cho, *Nano Lett.*, **15**, 2111 (2015).
23. M. Yoon, Y. Dong, J. Hwang, J. Sung, H. Cha, K. Ahn, Y. Huang, S. J. Kang, J. Li and J. Cho, *Nat. Energy*, **6**, 362 (2021).
24. S. Yubuchi, Y. Ito, T. Matsuyama, A. Hayashi and M. Tatsumisago, *Solid State Ion.*, **285**, 79 (2016).
25. H. Lee, P. Oh, J. Kim, H. Cha, S. Chae, S. Lee and J. Cho, *Adv. Mater.*, **31**, 1900376 (2019).
26. R. Koerver, I. Aygün, T. Leichtweiß, C. Dietrich, W. Zhang, J. O. Binder, P. Hartmann, W. G. Zeier and J. r. Janek, *Chem. Mater.*, **29**, 5574 (2017).
27. N. Machida, J. Kashiwagi, M. Naito and T. Shigematsu, *Solid State Ion.*, **225**, 354 (2012).
28. K. Okada, N. Machida, M. Naito, T. Shigematsu, S. Ito, S. Fujiki, M. Nakano and Y. Aihara, *Solid State Ion.*, **255**, 120 (2014).
29. Y. Seino, T. Ota and K. Takada, *J. Power Sources*, **196**, 6488 (2011).
30. S. Ito, S. Fujiki, T. Yamada, Y. Aihara, Y. Park, T. Y. Kim, S.-W. Baek, J.-M. Lee, S. Doo and N. Machida, *J. Power Sources*, **248**, 943 (2014).
31. H. S. Ko, H. W. Park, G. J. Kim and J. D. Lee, *Korean J. Chem. Eng.*, **36**, 620 (2019).
32. H. S. Ko, J. H. Kim, J. Wang and J. D. Lee, *J. Power Sources*, **372**, 107 (2017).
33. M. Dong, Z. Wang, H. Li, H. Guo, X. Li, K. Shih and J. Wang, *ACS Sustain. Chem. Eng.*, **5**, 10199 (2017).
34. P. Yan, J. Zheng, X. Zhang, R. Xu, K. Amine, J. Xiao, J.-G. Zhang and C.-M. Wang, *Chem. Mater.*, **28**, 857 (2016).
35. Q. Li, W. Zhuang, Z. Li, S. Wu, N. Li, M. Gao, W. Li, J. Wang and S. Lu, *ChemElectroChem*, **7**, 998 (2020).
36. J. Chen, H. Yang, T. Li, C. Liu, H. Tong, J. Chen, Z. Liu, L. Xia, Z. Chen and J. Duan, *Front. Chem.*, **7**, 500 (2019).